

# Laser-assisted morphing of complex three dimensional objects

Jakub Drs,<sup>1,\*</sup> Tetsuo Kishi,<sup>2</sup> Yves Bellouard<sup>1</sup>

<sup>1</sup>Galatea Laboratory, STI/IMT, Ecole Polytechnique Fédérale de Lausanne (EPFL), Neuchâtel, Switzerland  
<sup>2</sup>Department of Chemistry and Materials Science, Tokyo Institute of Technology, 2-12-1 Ookayama Meguro-ku,  
Tokyo, Japan

\*[jakub.drs@epfl.ch](mailto:jakub.drs@epfl.ch)

**Abstract:** Morphing refers to the smooth transition from a specific shape into another one, in which the initial and final shapes can be significantly different. A typical illustration is to turn a cube into a sphere by continuous change of shape curvatures. Here, we demonstrate a process of laser-induced morphing, driven by surface tension and thermally-controlled viscosity. As a proof-of-concept, we turn 3D glass structures fabricated by a femtosecond laser into other shapes by locally heating up the structure with a feedback-controlled CO<sub>2</sub> laser. We further show that this laser morphing process can be accurately modelled and predicted.

©2015 Optical Society of America

**OCIS codes:** (140.3390) Laser materials processing; (160.6030) Silica; (320.2250) Femtosecond phenomena; (320.7130) Ultrafast processes in condensed matter, including semiconductors; (220.4000) Microstructure fabrication; (140.3470) Lasers, carbon dioxide.

---

## References and Links

1. A. Marcinkevičius, S. Juodkazis, M. Watanabe, M. Miwa, S. Matsuo, H. Misawa, and J. Nishii, "Femtosecond laser-assisted three-dimensional microfabrication in silica," *Opt. Lett.* **26**(5), 277–279 (2001).
2. Y. Cheng, H. L. Tsai, K. Sugioka, and K. Midorikawa, "Fabrication of 3D micro optical lenses in photosensitive glass using femtosecond laser micromachining," *Appl. Phys. A*, **85**, 11–14 (2006).
3. Y. Bellouard, A. Said, M. Dugan, and P. Bado, "Fabrication of high-aspect ratio, micro-fluidic channels and tunnels using femtosecond laser pulses and chemical etching," *Opt. Express* **12**(10), 2120–2129 (2004).
4. K. M. Davis, K. Miura, N. Sugimoto, and K. Hirao, "Writing waveguides in glass with a femtosecond laser," *Opt. Lett.* **21**(21), 1729–1731 (1996).
5. K. Minoshima, A. Kowalevicz, E. Ippen, and J. Fujimoto, "Fabrication of coupled mode photonic devices in glass by nonlinear femtosecond laser materials processing," *Opt. Express* **10**(15), 645–652 (2002).
6. Y. Bellouard, A. Said, and P. Bado, "Integrating optics and micro-mechanics in a single substrate: a step toward monolithic integration in fused silica," *Opt. Express* **13**(17), 6635–6644 (2005).
7. Y. Bellouard, A. Said, M. Dugan, and P. Bado, "Monolithic three-dimensional integration of micro-fluidic channels and optical waveguides in fused silica," *Proc. MRS* **782**, 63–68 (2003).
8. A. Schaap and Y. Bellouard, "Molding topologically-complex 3D polymer microstructures from femtosecond laser machined glass," *Opt. Mater. Express* **3**(9), 1428–1437 (2013).
9. V. Tielen and Y. Bellouard, "Three-dimensional glass monolithic micro-flexure fabricated by femtosecond laser exposure and chemical Etching," *Micromachines* **5**(3), 697–710 (2014).
10. P. A. Temple, W. H. Lowdermilk, and D. Milam, "Carbon dioxide laser polishing of fused silica surfaces for increased laser-damage resistance at 1064 nm," *Appl. Opt.* **21**(18), 3249–3255 (1982).
11. Y. M. Xiao and M. Bass, "Thermal stress limitations to laser fire polishing of glasses," *Appl. Opt.* **22**(18), 2933–2936 (1983).
12. F. Laguarda, N. Lupon, and J. Armengol, "Optical glass polishing by controlled laser surface-heat treatment," *Appl. Opt.* **33**(27), 6508–6513 (1994).
13. F. Laguarda, N. B. Lupon, F. Vega, and J. Armengol, "Laser application for optical glass polishing," in *Optical Instrumentation & Systems Design* (International Society for Optics and Photonics, 1996), pp. 603–610.
14. M. Udrea, H. Orun, and A. Alacakar, "Laser polishing of optical fiber end surface," *Opt. Eng.* **40**(9), 2026–2030 (2001).
15. D. K. Armani, T. J. Kippenberg, S. M. Spillane, and K. J. Vahala, "Ultra-high-Q toroid microcavity on a chip," *Nature* **421**(6926), 925–928 (2003).
16. M. D. Feit and A. M. Rubenchik, "Mechanisms of CO<sub>2</sub> laser mitigation of laser damage growth in fused silica," *Proc. SPIE* **4932**, 91–102 (2003).

17. S. Calixto, M. Rosete-Aguilar, F. J. Sanchez-Marin, and L. Castañeda-Escobar, "Rod and spherical silica microlenses fabricated by CO<sub>2</sub> laser melting," *Appl. Opt.* **44**(21), 4547–4556 (2005).
18. K. M. Nowak, H. J. Baker, and D. R. Hall, "Efficient laser polishing of silica micro-optic components," *Appl. Opt.* **45**(1), 162–171 (2006).
19. C. Kim, I.-B. Sohn, Y. J. Lee, C. C. Byeon, S. Y. Kim, H. Park, and H. Lee, "Fabrication of a fused silica based mold for the microlenticular lens array using a femtosecond laser and a CO<sub>2</sub> laser," *Opt. Mater. Express* **4**(11), 2233–2240 (2014).
20. J. Tang, J. Lin, J. Song, Z. Fang, M. Wang, Y. Liao, L. Qiao, and Y. Cheng, "On-chip tuning of the resonant wavelength in a high-Q microresonator integrated with a microheater," *Int. J. Optomech.* **9**(2), 187–194 (2015).
21. W. D. Kingery, "Thermal conductivity: XII, Temperature dependence of conductivity for single-phase ceramics," *J. Am. Ceram. Soc.* **38**(7), 251–255 (1955).
22. K. L. Wray and T. J. Connolly, "Thermal conductivity of clear fused silica at high temperatures," *J. Appl. Phys.* **30**(11), 1702–1705 (1959).
23. S. T. Yang, M. J. Matthews, S. Elhadj, V. G. Draggoo, and S. E. Bisson, "Thermal transport in CO<sub>2</sub> laser irradiated fused silica: In situ measurements and analysis," *J. Appl. Phys.* **106**(10), 103106 (2009).
24. P. Combis, P. Cormont, L. Gallais, D. Hebert, L. Robin, and J.-L. Rullier, "Evaluation of the fused silica thermal conductivity by comparing infrared thermometry measurements with two-dimensional simulations," *Appl. Phys. Lett.* **101**(21), 211908 (2012).
25. R. H. Doremus, "Viscosity of silica," *J. Appl. Phys.* **92**(12), 7619–7629 (2002).
26. Heraeus Quarzglas - Thermal properties," [http://heraeus-Quarzglas.com/en/quarzglas/thermalproperties/Thermal\\_properties.aspx](http://heraeus-Quarzglas.com/en/quarzglas/thermalproperties/Thermal_properties.aspx).
27. K. Boyd, H. Ebendorff-Heidepriem, T. M. Monro, and J. Munch, "Surface tension and viscosity measurement of optical glasses using a scanning CO<sub>2</sub> laser," *Opt. Mater. Express* **2**(8), 1101–1110 (2012).
28. P. Bouchut, D. Decruppe, and L. Delrive, "Fused silica thermal conductivity dispersion at high temperature," *J. Appl. Phys.* **96**(6), 3221–3227 (2004).
29. A. D. McLachlan and F. P. Meyer, "Temperature dependence of the extinction coefficient of fused silica for CO<sub>2</sub> laser wavelengths," *Appl. Opt.* **26**(9), 1728–1731 (1987).
30. M. Lancry, E. Régner, and B. Poumellec, "Fictive temperature in silica-based glasses and its application to optical fiber manufacturing," *Prog. Mater. Sci.* **57**(1), 63–94 (2012).
31. A. Agarwal and M. Tomozawa, "Correlation of silica glass properties with the infrared spectra," *J. Non-Cryst. Solids* **209**(1-2), 166–174 (1997).
32. M. Cai, O. Painter, K. J. Vahala, and P. C. Sercel, "Fiber-coupled microsphere laser," *Opt. Lett.* **25**(19), 1430–1432 (2000).
33. T. Kumagai, T. Kishi, and T. Yano, "Low threshold lasing of bubble-containing glass microspheres by non-whispering gallery mode excitation over a wide wavelength range," *J. Appl. Phys.* **117**(11), 113104 (2015).
34. R. Kitamura, L. Pilon, and M. Jonasz, "Optical constants of silica glass from extreme ultraviolet to far infrared at near room temperature," *Appl. Opt.* **46**(33), 8118–8133 (2007).
35. O. Rozenbaum, D. D. S. Meneses, Y. Auger, S. Chermanne, and P. Echegut, "A spectroscopic method to measure the spectral emissivity of semi-transparent materials up to high temperature," *Rev. Sci. Instrum.* **70**(10), 4020–4025 (1999).

## 1. Introduction

### 1.1 The concept of morphing

The idea of morphing is based on the existence of a smooth transformation between two different shapes of an object. The term is popularized as a visual effect in film production to depict a person's face magically turning into another one. The transition between the two character's faces is seamless, keeping the same general facial features throughout the transformation. Here, we use this analogy to depict a fabrication process where a given initial shape is gradually transformed into another, radically different shape, using physical processes to drive the smooth transformation between the two.

As an illustration (see Fig. 1), let us consider a cube that is heated so that its viscosity decreases. Surface tension will gradually turn the object into a sphere, which in this case corresponds to a minimum surface energy. This is just an example. The concept can be generalized to any force field capable of shaping a viscous volume of matter.

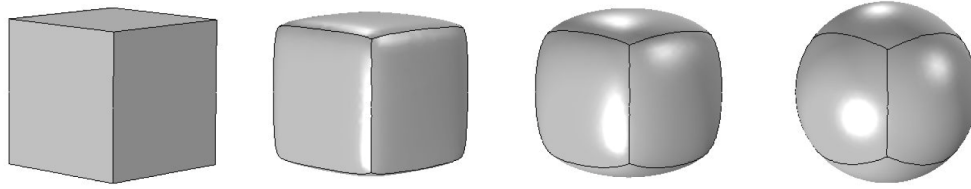


Fig. 1. Illustration of the concept of shape morphing. A cube is turning into a sphere by seamless transformation.

In micromanufacturing, the concept of morphing driven by surface tension is attractive for multiple reasons. First, the final shape will absorb shape imperfections that may be present in the original. Parameters such as surface roughness and/or waviness are no longer relevant, since this fine level of detail will disappear. In particular, optical components such as resonators require levels of surface quality that cannot easily be achieved using traditional machining approaches. Second, some shapes are impossible to realize through known direct machining methods. A typical example is a volume enclosing a void with optical surface quality. As we will demonstrate throughout this paper, shape morphing offers a possible route for fabricating these objects.

### *1.2 A possible route for implementing surface-tension driven shape morphing*

To implement surface tension driven shape morphing, we propose to combine femtosecond laser, three-dimensional machining techniques, with feedback-controlled CO<sub>2</sub> laser heating.

#### *1.2.1 3D manufacturing using femtosecond lasers and chemical etching*

Femtosecond laser exposure combined with chemical etching [1–3] has emerged over the last decade as an efficient manufacturing technique for fabricating a variety of three-dimensional shapes. These include devices combining multiple functionalities, such as optical waveguides [4,5], mechanical functions [6] and fluidics [7]. The typical fabrication procedure consists of first, exposing the material to femtosecond radiation at an energy level where the material structure is modified but no ablation takes place and second, performing a chemical etching step using HF or KOH etchants. Using this process, arbitrary three-dimensional shapes can be created that form the basis for complex structures such as molds [8] or three-dimensional flexures [9].

#### *1.2.2 Controlled viscosity in glass using CO<sub>2</sub> lasers*

As tool for melting material, CO<sub>2</sub> lasers have been used in a variety of applications since the early 80s. Various application examples include optical polishing [10–18], fabrication of toroidal optical resonators [15], repair of laser-induced damage in optical components [16], fabrication of micro-lenses [17,18], and glass mold fabrication for micro-lenses arrays [19]. Recently [20], CO<sub>2</sub> laser controlled melting was also used in combination with femtosecond laser fabrication to produce structures similar to those reported in [15], but in an all-glass substrate.

In this study, we show that CO<sub>2</sub> laser melting combined with three-dimensional femtosecond laser micromachining offers an opportunity to implement shape morphing. We demonstrate the potential of this technique for future applications by applying it to a shape with a complex topology, leading to a self-sealed cavity. Unlike previous works, we further demonstrate a full model of the dynamic evolution of a shape during laser exposure. Finally, we show that this model is in good agreement with observations and is applicable to any arbitrary object geometry.

## 2. Experiments: feedback controlled CO<sub>2</sub> laser heating

A key requirement for achieving repeatable and accurate results is to implement a feedback loop in order to maintain a constant temperature in the system. A schematic of the optical and mechanical assembly is shown in Fig. 2. A CO<sub>2</sub> laser (SYNRAD Firestar ti80) irradiates the sample through a ZnSe focusing lens ( $f = 50$  mm). The laser profile was measured at the sample plane using a knife-edge technique and was found to be Gaussian with radius of 300  $\mu\text{m}$  ( $1/e^2$  diameter). To compensate for fluctuations in the laser output power (about  $\pm 7\%$ ), a PID controller was implemented, using an IR temperature measurement from the specimen for feedback. The performance of the controller exhibited zero overshoot and a rise time of about 200 ms. Mean error from the constant reference was typically less than 0.1%. The feedback signal was provided by an InGaAs photodiode (Thorlabs, DET410) with a spectral sensitivity window spanning from 800 to 1700 nm. Although the temperature was not measured directly, the closed-loop guarantees a perfect temperature stability and very good repeatability of the experiments. An indirect estimate based on the numerical model (to be outlined later) is that the *temperature* stability achieved during experiments was about  $\pm 1\%$ . The laser power ranged from 8 to 14 W with an exposure time of 0.5 to 60 s.

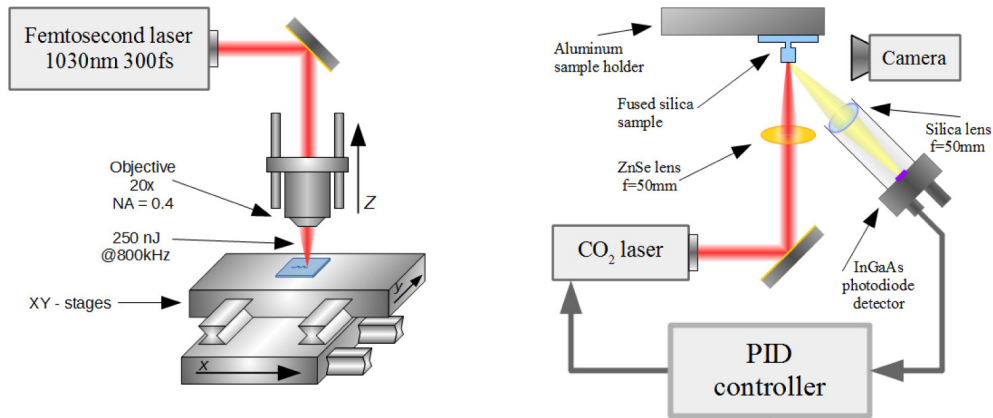


Fig. 2. Laser platforms used for the fabrication. Fused silica patterns are fabricated by femtosecond laser exposure (left) followed by wet etching in HF. After this process, the microstructures are introduced onto the CO<sub>2</sub> platform (right) for shape morphing.

A CMOS camera (acquisition rate of 25 frames per second) equipped with a 20x telecentric objective (Moritex-Schott SOD-10X + 2X) was used to observe a side-view of the evolution of the microstructure shape during CO<sub>2</sub> laser exposure, providing an accurate profile measurement during the morphing process.

The sample holder was made of aluminum with relatively large dimensions compared to the sample, resulting in a very good heat sink at the bottom of the specimen, giving a constant temperature reference. OH-rich (>1000 ppm) synthetic fused silica was used as substrate for the experiments. The sample patterns were fabricated in a 250  $\mu\text{m}$ -thick substrate using the process described in [7]. Laser exposure was performed using an Ytterbium-fiber based femtosecond laser (Amplitude Systèmes), emitting 270 fs pulses at a rate of 400 kHz and pulse energy of 220 nJ.

## 3. Numerical modelling

To model and predict the final shape during CO<sub>2</sub> exposure, a numerical model was developed, putting emphasis on applicability to arbitrary object geometry. A three-dimensional finite element analysis model was chosen; covering both the surface tension driven flow and heat transfer in the material. This model was implemented using a commercially available software

(COMSOL Multiphysics). Two predefined segregated solvers, optimized for the fluid flow and heat transfer, were used on a common deformable mesh following the object shape. The heat transfer solver uses quadratic elements by default while the fluid flow solver employs linear elements for both pressure and velocity. These two solvers are iterated at each time step until the criteria for all dependent variables tolerance is satisfied.

The coupled problem is defined by the following set of partial differential equations:

$$\begin{cases} \rho C_p(T) \left[ \frac{\partial T}{\partial t} + \mathbf{u} \cdot \nabla T \right] = \nabla \cdot [k(T) \nabla T] + Q(\mathbf{x}, t) \\ \rho \frac{\partial \mathbf{u}}{\partial t} = \nabla \cdot \left\{ -p \mathbf{I} + \mu(T) \left[ \nabla \mathbf{u} + (\nabla \mathbf{u})^T \right] \right\} + F(\mathbf{x}, t) \\ \rho \nabla \cdot \mathbf{u} = 0 \end{cases} \quad (1)$$

In this set of equations, the dependent variables are the temperature  $T$ , the flow velocity  $\mathbf{u}$ , and the pressure  $p$ , respectively. The external heat  $Q(\mathbf{x}, t)$  is related to laser irradiation and cooling of the system and an external force  $F(\mathbf{x}, t)$  accounts for the surface tension. The other parameters are the material density  $\rho$ , specific heat  $C_p(T)$ , thermal conductivity  $k(T)$ , and viscosity  $\mu(T)$ .

One of the difficulties here is that most of these material properties are strongly temperature dependent. Even though fused silica is one of the most investigated materials, the temperature dependent properties are not always consistent in the literature. For example, the thermal conductivity exhibits a significant discrepancy above 1000 °K. Kingery [21] claims that the thermal conductivity of fused silica rises rapidly above this limit, while other authors [22, 23] have reported that the conductivity approaches a constant value above 2000 °K. Finally, Combis *et al.* [24] observed a significant conductivity drop between 1500 and 2000 °K. A similar variability could be found for the viscosity, as stated in [25].

In this study, we decided to use the data provided by the manufacturer (Heraeus [26]) for synthetic fused silica, in particular to fit an Arrhenius model to capture the thermal dependence of viscosity, as follows:

$$\mu(T) = \mu_0 e^{\frac{A}{R \cdot T}} \quad \text{with} \quad \mu_0 = 8.31 \cdot 10^{-9} \text{ [Pa} \cdot \text{s]} \quad \text{and} \quad A = 5.26 \cdot 10^5 \left[ \frac{1}{\text{J} \cdot \text{mol}} \right]. \quad (2)$$

For the specific heat and thermal conductivity, an interpolation function was used in the model. The surface tension is not provided so we have used the value of  $\sigma = 0.3 \text{ N/m}$  measured by Boyd *et al.* [27]. The parameters used in this simulation are further described in the appendix (see Table 1).

The next step in this modeling is the definition of the boundary conditions. For the heat transfer equation, there are four main contributors: The first is a heat source that depends on the beam profile, laser power, and the shape of the object to be heated. The beam profile was Gaussian and, together with the laser power, was measured experimentally. The absorption of the laser light was modeled as a surface phenomenon, due to the high absorption of fused silica at 10.6  $\mu\text{m}$ . In this case, the penetration depth is negligible compared to the area covered by the beam. The absorption is modeled using Fresnel's equations, as follows:

$$P_{\text{abs}}(x, t) = \left[ 1 - R(n_{\text{silica}}, \theta_{x,t}) \right] P_{\text{laser}}(x, t). \quad (3)$$

The reflectivity coefficient  $R$  is mainly dependent on the incidence angle of the laser light and refractive index of fused silica. The other three contributors to the heat transfer boundary conditions are related to the system cooling: cooling due to the ambient air, radiation losses, and thermal contact with the sample holder. Of these three, the most significant factor is the thermal contact, which was modeled as 5- $\mu\text{m}$  air gap between the

specimen and a perfect heat sink at 300 K (the heat sink used in the experiment was coarse-polished, black-anodized aluminum).

For modeling the glass flow (as a viscous fluid), only one boundary condition is related to the external force  $Q(\mathbf{x}, t)$ , which in our case is the surface tension.

To accurately compare the numerical model with the experiments, the CO<sub>2</sub> laser was kept under closed-loop control (PID) using an IR diode as feedback so that the average temperature of the specimen was constant, though a temperature gradient was still present. To best match the model with experimental conditions, a fixed temperature boundary was not used, but rather the feedback loop was simulated in the numerical model. The irradiance was then modeled in a very similar way as it was in the experiment, i.e. the irradiance level is adjusted according to the mean temperature in the system until a referenced value is reached. This method enables virtual, stable regulation of the average temperature in the system (as it is during the experiment) while not disturbing the temperature *distribution* by enforcing a constant temperature boundary condition.

The agreement with the experimental dynamics shows the efficiency of this approach, since it effectively compensates small nuances between the model and reality, and makes the simulation particularly robust to small variations of the starting conditions.

#### 4. Results and discussions

For the experiments, we consider two test shapes, illustrated in Fig. 3, which were micromachined in fused silica using femtosecond laser machining combined with chemical etching according to the process described in [3]. The first shape is a cube sitting on a pillar. The objective is to demonstrate the ability to fabricate a small supported sphere that can act as a micro-lens or whispering-gallery-mode optical resonator. The second shape is a cylinder with a conical cavity in the middle. Here the objective is to demonstrate that this morphing technique can be used to change the surface topology, creating a sealed cavity. One could imagine using this concept for trapping a gas for applications such as a gas reference cell for a miniaturized atomic clock.

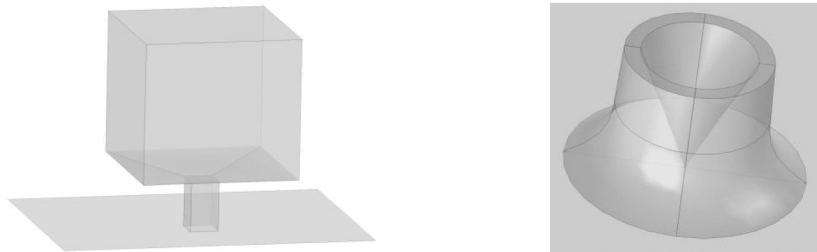


Fig. 3. Fused silica patterns used in the CO<sub>2</sub> laser shape morphing experiments. A cube (100 micron square) seated on a pillar (left) and a round pillar (100 micron diameter) with a conical cavity (right).

##### 4.1 Case 1. From a cube to a sphere

In addition of demonstrating the concept of morphing, we also seek to show agreement between experimental observation and the derived model, and in particular, the ability of the model to capture the dynamic evolution of the shape morphology during heating. For this purpose, recorded video plays a major role since it captures the dynamics of the morphing process in real-time. For fitting the numerical model with the experiment, we have chosen to use the mean temperature as the unique tuning parameter (see previous discussion).

Assuming the average temperature is stable throughout the morphing process, we have found an excellent agreement between the actual shapes and the modeled ones at various time steps as shown in Figs. 4 and 5, demonstrating that the model effectively captures the dynamics of the morphing process.



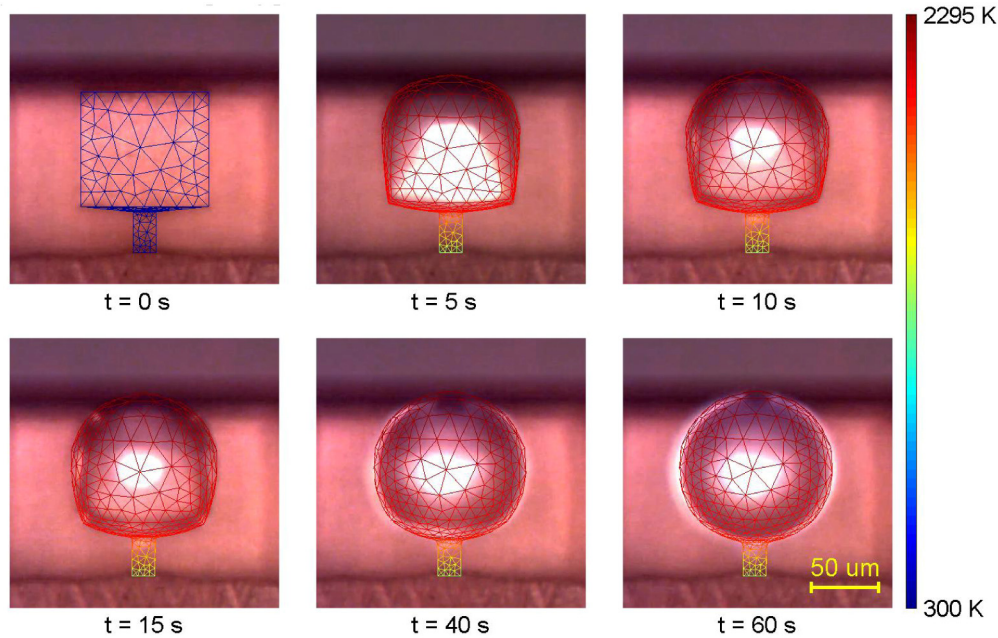


Fig. 4. Still frames taken from video footage of the morphing process merged with the numerical model at fixed time intervals. The scale bar on the right corresponds to the mesh color and indicates the temperature. The model accurately covers the whole morphing process, including melting of the pillar, as shown in the last picture. ([Visualization 1](#))

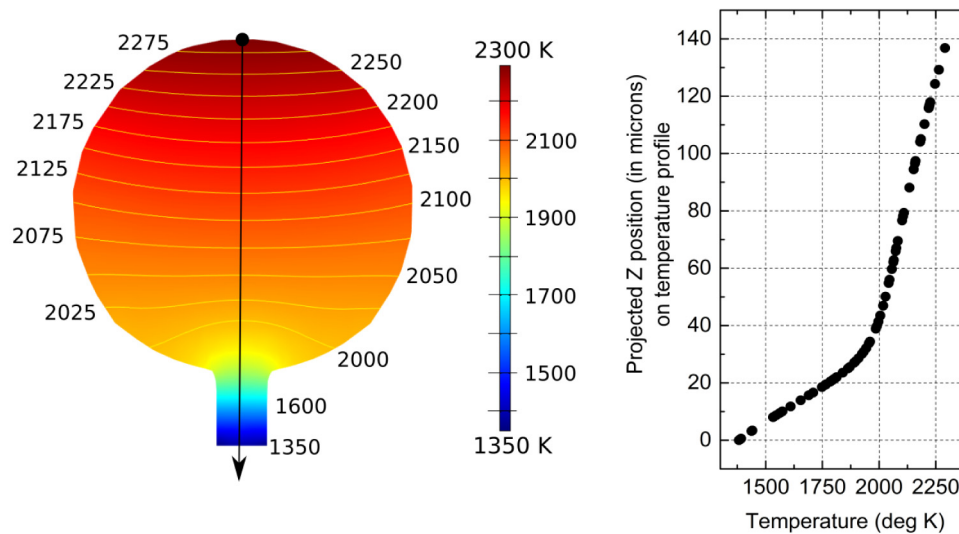


Fig. 5. Thermal gradient across the microsphere simulated after 60s of heating time (see Fig. 4). The laser was incident on the top of the sphere. Left: Simulated thermal distribution on a projected transverse plane. Right: Simulated surface temperature profile projected along the z-axis.

In practice, there are many influencing factors affecting the process dynamics, such as fluctuations in the emitted laser power, small specimen misalignment, nonhomogeneous thermal conductivity [28], as well as the temperature dependence of extinction coefficient for fused silica [29]. These inherent process fluctuations are not easily predictable, however their influence can be effectively compensated using feedback-controlled laser heating, as

illustrated in Fig. 6, which shows still images for *four* different specimens, taken after the same exposure time ( $\pm 0.2$  s).

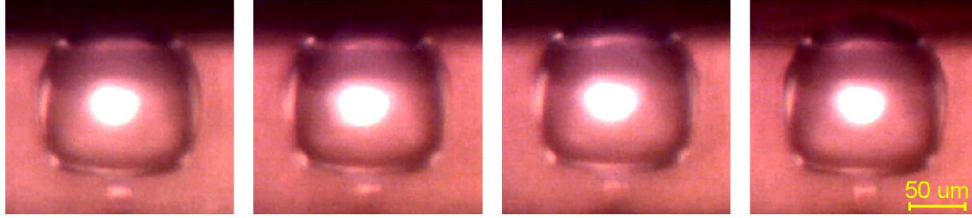


Fig. 6. Experimental reproducibility showing the resulting shape of four consecutive experiments. The pictures have been taken after 20 s ( $\pm 0.2$  s) of morphing at 2300 K.

In the model, two indirect links with the real temperature can be inferred. The first is the morphing dynamics that are driven by surface tension, which is directly related to the temperature-dependent viscosity of the glass. The second link refers to the laser irradiance, which is related to the heat transfer in the system. The first link, i.e. the dynamic evolution of the shape morphology, has been used to fit the model to experimental observation, while the second was confronted with the experimental data. After calibrating the model at different temperatures, the simulated and measured value of laser irradiance was found to stay within a 15% tolerance, suggesting a good fidelity between the model and experiments. This is due to the fact that the implemented PID control loop maintains a constant temperature during heating with the CO<sub>2</sub> laser.

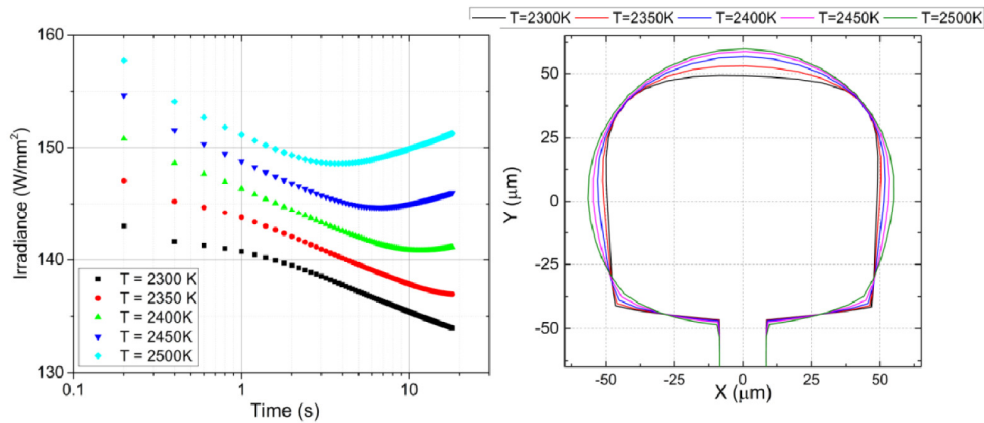


Fig. 7. Simulation of the morphing of a cube for different temperature set points. The left image depicts the laser irradiance evolution in time, while the right image shows the corresponding object profile after a heating time of 2 s for various set point temperatures. The profile corresponds to the yz-plane of the 3D model.

With a good fit of the numerical, we can test the importance of certain parameters on the morphing technique. Figure 7 shows the irradiance level evolution in time during laser exposure, as well as the shape obtained after 2 s for a given maximum temperature set point. The time-dependent irradiance exhibits two noticeable regimes. In the first regime, the initial heating of the material takes place, which is dependent on the specific heat. This transient regime is typically very fast for the volume considered (about 100 microns cube), with a time constant of about 100 ms. The second regime is driven by the glass viscosity, and accounts for the morphing process itself. This process is much slower, typically lasting for several seconds depending on the set temperature in the PID loop. In this regime, the laser irradiance decreases gradually. This variation is due to the larger laser exposed area of a sphere in



contrast to the original cube. This change is compensated by the controller which leads to the lower laser irradiance to maintain a constant temperature.

The final irradiance rise, which is visible at higher temperatures, is related to the melting of the supporting pillar, lowering of the thermal resistance of heat to flow toward the cooled, bottom region of the substrate.

The simulation also shows that the differences between reachable object shapes at different temperatures are nearly negligible. This means that a same object shape can be produced at various temperatures by adjusting the exposure time properly. However, it is still important to optimize the temperature. Due to the fast cooling rate of the system (typical time constant of 100 ms), different fictive temperatures, and therefore different properties for the final object [30], such as refractive index [31], can be obtained, depending on the maximum temperature from which the object melt started.

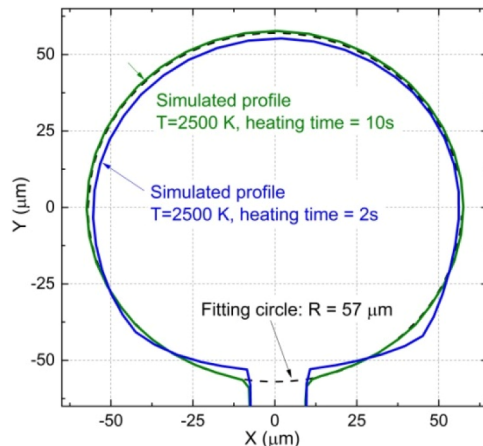


Fig. 8. Simulated profile fitted with a circle of  $57\ \mu\text{m}$  in radius. The profile is taken at  $T = 2500\ \text{K}$  after a laser heating time of 2s and 10s. As can be seen, the heated profile converges toward a nearly perfect circle after 2s, though some slight distortion can be seen along the negative y direction (this is the coolest zone since the structure is heated from the top by the laser). This distortion disappears after a sufficient heating time (10s in this case).

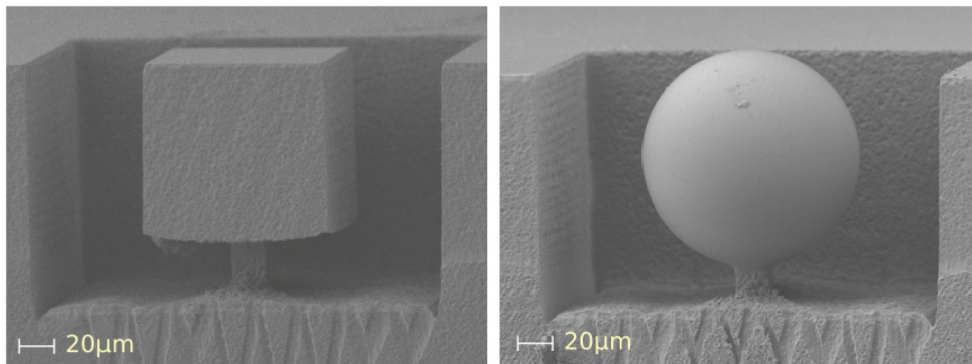


Fig. 9. Scanning Electron Microscope images demonstrating the concept of laser morphing (in this case, turning a cube into a sphere). The left image shows a cube, after femtosecond laser exposure and chemical etching, but before heating. The image on the right shows a similar cube after morphing, illustrating the perfect surface quality and sphericity achieved. (The V-marks at the bottom of the images are labels for identification purpose.)

Figure 8 shows that nearly perfect circular profile can be obtained after a few seconds of heating. Since gravity plays virtually no role at this scale, perfect spherical profiles

corresponding to the lowest surface energy can be achieved. A dramatic illustration is further shown in the SEM images presented in Fig. 9. The first image is a cube after femtosecond laser exposure and chemical etching. The second image shows a similar cube turned into a perfect sphere with sub-nanometer roughness after laser morphing.

#### 4.2 Case 2. From a cylinder with a cone toward a sealed cavity

As an illustration of a more complex shape morphing, we now consider a cylinder with a conical cavity. In this case, the morphing process is much less intuitive than in the case we considered in the previous section.

The shape evolution of the conical cavity is depicted in Fig. 10. The cavity self-seals during laser exposure, capturing the surrounding gas inside. The corresponding result of our simulation is shown in Fig. 11. Unfortunately, we are not able to simulate the coalescence of the top of the cylinder, because the surface is modeled with a moving mesh, which cannot change topology during simulation. However, our model properly simulates the evolution of the shape up to the point where the cavity nearly seals itself.

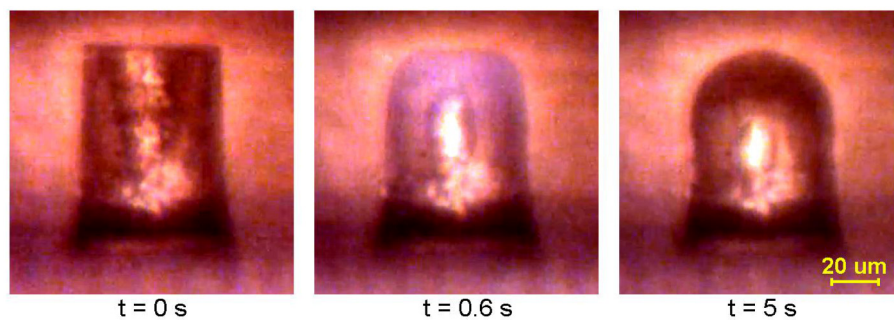


Fig. 10. Capture of a gas bubble in a glass microstructure containing a conical cavity, which is sealed during the process of laser exposure and structural morphing. The sealed cavity is clearly visible in the middle of the last picture. ([Visualization 2](#))

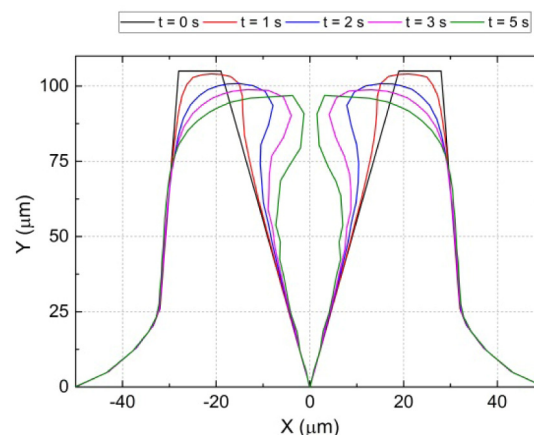


Fig. 11. Simulation of the closing of a conical cavity at various time steps. Although the merging of the interface could not be simulated, the model efficiently captures the evolution of the structure during the morphing process and predicts the sealing of the initially open cavity. After temperature calibration, the simulated laser power differed from the measured value by only 3%, thus further demonstrating the accuracy of the model.

The simulation results were also compared with actual profilometry data obtained from experiments before closing of the cavity (Fig. 12). The simulation was aligned the same way as in case of the cube and we again observed a good conformity with the experiment. The

profilometry covers only part of the surface where the slope is sufficiently small to be visible on a confocal profilometer.

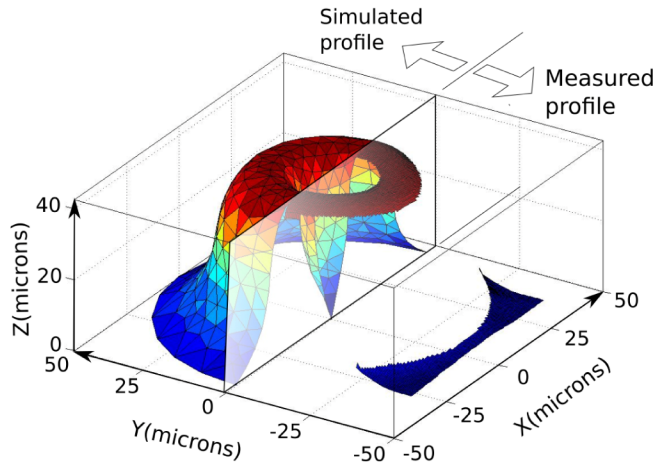


Fig. 12. Comparison between the simulated shape (left side) and profilometry data (right) for a pillar with a conical cavity with a diameter of  $\sim 50 \mu\text{m}$ , after a heating time of 8s at 2120 K. The profilometry data was obtained using a white-light interferometer.

## 5. Conclusion

In this paper, we have introduced the concept of laser morphing. This concept was tested in the case of surface-tension driven morphing by first machining an arbitrary three-dimensional shape using femtosecond laser exposure and chemical etching, and second, by heating the microstructures with a  $\text{CO}_2$  laser until they converge toward the desired final shape. This morphing technique brings practical benefits, such as an ultra-smooth surface, effective forming of spherical shapes, as well as the ability to change the surface topology in order to create ‘impossible’ objects like self-sealed cavities.

The proposed feedback-controlled laser heating system, combined with a temperature-calibrated 3D numerical model, shows that this technique can be accurately controlled and predicted. This model further allows for effective optimization of the process on arbitrary geometry.

As a proof of concept, we have demonstrated the morphing of a cube into a well-defined glass microsphere, supported by a small pillar. Additionally, we have also shown an example of morphing with higher complexity shape that resulted in a self-sealing cavity, illustrating a dynamic change of surface topology. In these examples perfect spheres can be used as optical resonators [32,33] while self-sealed cavities offer an efficient means for capturing small volumes of gas.

## Appendix:Table 1

Table 1. Parameters for fused silica used in this study for simulating the dynamical structural changes.

Symbol	Name	Expression	Source
$C_p(T)$	Thermal capacity	Interpolation function	[26]
$k(T)$	Thermal conductivity	Interpolation function	[26]
$\mu(T)$	Viscosity	$a \cdot e^{\frac{b}{R \cdot T}}$ [Pa · s] with $a = 8.31 \cdot 10^{-9}$ , $b = 5.26 \cdot 10^5$	[26]
$\Sigma$	Surface tension	0.3 [Nm]	[27]
$n_{10.6}$	Refractive index at 10.6 $\mu\text{m}$	2.2	[34]
$E(T)$	Surface emissivity	Interpolation function	[35]

## **Acknowledgment**

The stay of Jakub Drs at EPFL was partially supported by Czech Technical University (CTU) under a MSc student exchange program. The project is supported by the European Research Council (ERC Stg Galatea - 307442). The Galatea Lab further acknowledges the sponsoring of Richemont International. The authors express their gratitude to Ben McMillen for the final proof-reading. In this work, JD performed the experiments as well as the simulations, TK participated in discussions and brainstorming about spherical resonators, YB designed and supervised the research and suggested the concept of laser shape morphing presented in this paper. YB and JD wrote the manuscript. All authors participated to the manuscript revisions and improvements.